International Journal of Plant Production
https://doi.org/10.1007/s42106-025-00357-z

RESEARCH

Temporal Mapping of Wheat Growth Traits Using Sentinel-2 and Empirical Models in Northern Iran

Roohollah Akbari[1] · Behnam Kamkar[2] · Parisa Alizadeh Dehkordi[3] · Hossein Kazemi[4]

Received: 12 May 2025 / Accepted: 16 July 2025

Abstract

Analyzing agricultural production systems by identifying the prominent factors affecting yield variations across regions can support new strategies for problem resolving in agroecosystems. Assessing the physiological status of crop fields offers valuable insights into the efficiency of these systems in terms of resource acquisition and utilization. This study investigates temporal changes in Crop Growth Rate (CGR), Leaf Area Index (LAI), and Net Assimilation Rate (NAR), and generates corresponding spatial maps using satellite images and mathematical models. It also compares these indicators across wheat fields in different watersheds to illustrate the physiological conditions of the crops. Additionally, the research aims to propose a reliable model for large-scale estimation of wheat leaf area. Our findings showed that empirical NDVI-based models for estimating LAI were less accurate than models relying on satellite-derived indices. Additionally, CGR did not reach its maximum potential in the study area, and the watershed basins exhibited diverse time-series patterns in terms of CGR and LAI. In contrast, NAR remained relatively stable across different basins. These results suggest that agronomic practices and breeding strategies aimed at enhancing leaf area development could assist farmers in reducing yield variability between watersheds and contribute to overall yield enhancement.

Keywords Crop growth · Sentinel-2 imagery · Vegetation indices · Wheat mapping · CGR

Abbreviations

CGR	Crop Growth rate
LAI	Leaf Area Index
NAR	Net Assimilation Rate

Introduction

Wheat, rice, and maize are the three primary staple crops, jointly contributing nearly 60% of global caloric intake (FAO, 2023; Palacios-Rojas et al., 2020). Among them, wheat alone accounts for about 18% of the global dietary energy supply (FAOSTAT, 2023), making it a critical crop for food security and rural livelihoods. Global wheat demand is projected to exceed 1.2 billion tonnes by 2050, driven by population growth, dietary shifts, and increasing food requirements (Foresight, 2011; Ray et al., 2019). Meeting this growing demand, while managing constraints like land degradation, water scarcity, and climate variability, requires precision in crop monitoring and management.

In Iran, Golestan Province is one of the most important wheat-producing regions, consistently ranking among the top five provinces in terms of total production. Despite its significance, substantial spatial variability in wheat yield exists across its diverse watershed basins. This variation is influenced by complex interactions among genotype, environment, and agronomic practices. Addressing this

✉ Behnam Kamkar
kamkar@um.ac.ir

[1] Department of Agronomy, Gorgan University of Agricultural Sciences and Natural Resources, Gorgan, Iran

[2] Department of Agrotechnology, Ferdowsi University of Mashhad, Mashhad, Iran

[3] Department of Agronomy, Faculty of Agriculture, University of Shahrekord, Shahrekord, Iran

[4] Department of Horticulture, Gorgan University of Agricultural Sciences and Natural Resources, Gorgan, Iran

Published online: 05 August 2025

variability is essential to narrowing yield gaps, optimizing resource use, and improving overall production efficiency.

Understanding wheat growth dynamics—particularly indicators such as Leaf Area Index (LAI), Crop Growth Rate (CGR), and Net Assimilation Rate (NAR)—is vital for diagnosing physiological performance and identifying growth-limiting factors. LAI quantifies canopy structure and is strongly linked to light interception, evapotranspiration, and biomass accumulation (Zhu et al., 2019). CGR reflects how efficiently crops convert absorbed light and nutrients into biomass over time (Wiegand & Richardson, 1990). NAR, derived as CGR divided by LAI, serves as an indicator of photosynthetic efficiency per unit leaf area (Kumar et al., 2024).

Traditional methods of LAI measurement are destructive and labor-intensive, limiting their applicability at large scales. In contrast, advances in remote sensing technologies—particularly with Sentinel-2 satellite data—now enable accurate, timely, and spatially continuous estimation of crop biophysical variables across large agricultural landscapes (Suliga et al., 2019; Yu et al., 2020; Liu et al., 2021). However, despite these advances, region-specific models and validations remain limited, especially in data-sparse regions like Golestan.

Over the past two decades, two main approaches have been used to estimate LAI from satellite data: (1) empirical or semi-empirical models based on statistical relationships between vegetation indices (VIs) and field-measured LAI, and (2) physical models based on Radiative Transfer Models (RTMs) (Yu et al., 2020). While VI-based empirical models such as the Normalized Difference Vegetation Index (NDVI), the Nonparametric LAI Estimator (NPLE), and the Exponential Model with Experimental Parameters (EMEP) offer simplicity and speed, their performance often varies with crop type, growth stage, and local conditions.

(1) evaluateDespite growing interest in using remote sensing for crop monitoring, a key research gap remains: How can we best utilize satellite-derived physiological indices like LAI, CGR, and NAR to assess and explain yield variability across different watershed basins? Current studies rarely integrate these parameters at regional scales to provide actionable insights into spatial performance differences and yield-limiting factors. Moreover, there is a lack of clarity on whether empirical models or direct spectral indices offer more reliable estimates of LAI and related physiological traits under diverse field conditions.

This study aims to address this gap by framing LAI, CGR, and NAR not merely as monitoring variables but as diagnostic tools to assess regional yield potential and identify management targets for more equitable and efficient wheat production across watersheds.

Accordingly, the main objectives of this study were to:

1. Evaluate the spatial and temporal patterns of LAI, CGR, and NAR across wheat fields in the watershed basins of Golestan Province using Sentinel-2 imagery;
2. (Compare the accuracy and reliability of empirical models (NPLE, EMEP) versus direct vegetation indices (e.g., NDVI) for LAI estimation at large scales;
3. (Analyze the relationships between field-measured LAI and CGR with satellite-derived indices across different growth stages;
4. (Identify key phenological stages and physiological constraints limiting CGR in specific regions, to inform more targeted and sustainable wheat management strategies.

By linking remotely sensed biophysical indicators with regional production disparities, this research aims to support both scientific understanding and practical decision-making for improving wheat productivity in Golestan Province and similar agro-ecological zones.

Materials and Methods

Study Region

This study was conducted during the 2020–2021 wheat growing season across ten eastern watershed basins in Golestan Province, Iran, including Zaringol, Ghorchai, Tilabad, Narmab, Chehelchai, Oghan, Madarsoo, Kalhaji, Yelcheshmeh, and Gharnaveh, covering a total area of approximately 7,450 km² (Fig. 1). The study area includes diverse land uses (forests, residential areas in the south and extensive croplands in central areas), with Five climate types — based on the De-Martonne classification—ranging from arid in the north to humid and semi-humid in the south—with annual precipitation varying between 250 and 700 mm. As a key rainfed agricultural area, Golestan which is among Iran's top wheat-producing provinces, ranking second in rainfed and sixth in irrigated wheat production in 2020–2021. Overall, it ranks fourth nationally in total wheat output (Statistical Center of Iran, 2021), supporting its selection as a representative site for regional wheat growth monitoring.

Fields Sampling and Laboratory Measurements

Initially, a comprehensive field survey was conducted across the study region, with 50 specific points within wheat fields (Fig. 1). Subsequently, over the course of the wheat growing season and spanning five distinct phenological stages, namely stem elongation (SE), middle ear emergence (MEE), late ear emergence (LEE), flowering

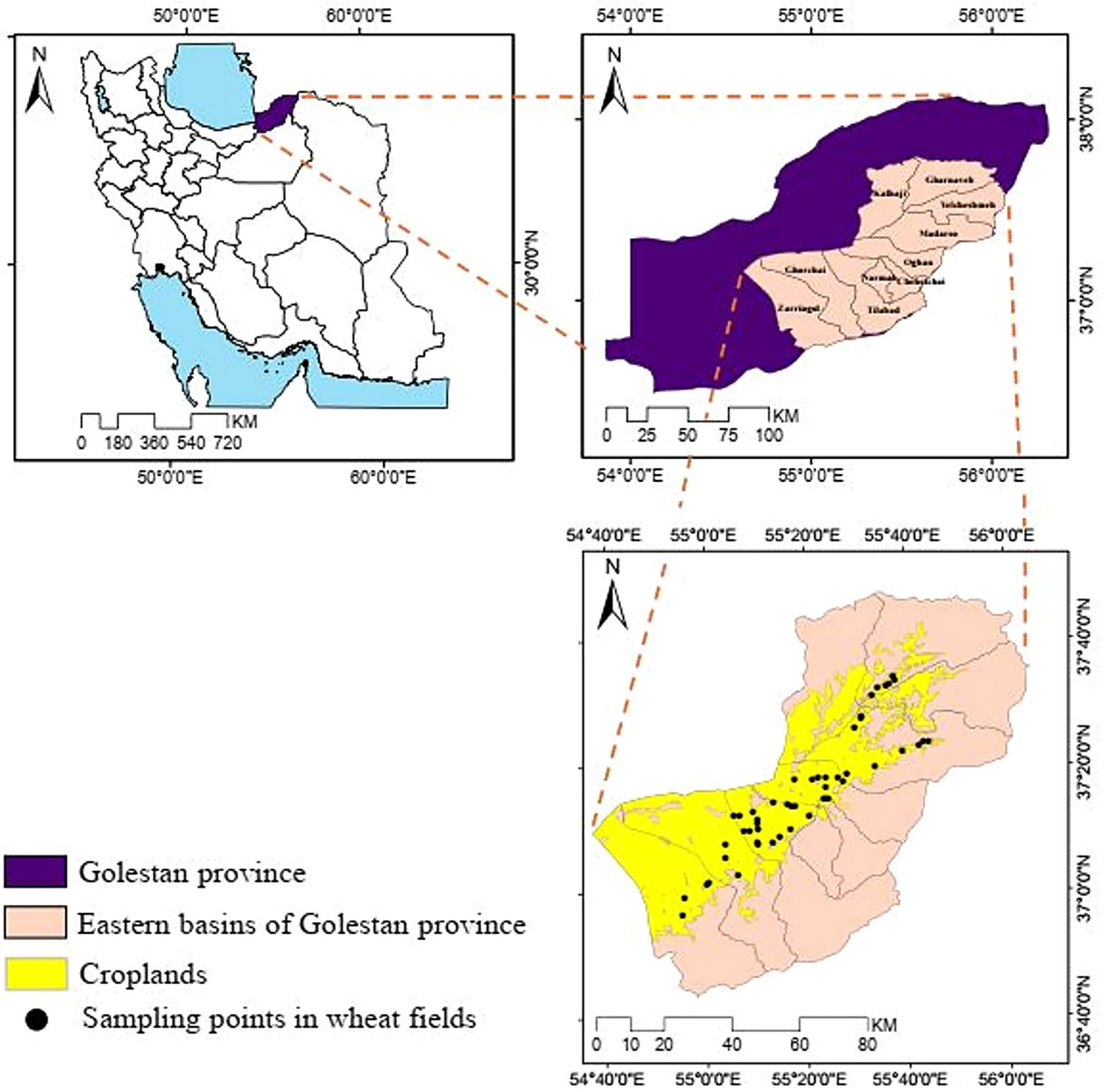

Fig. 1 Location of the study area in Golestan Province, Iran, showing the spatial distribution of ground sampling sites

(FL), and milk development (MD) using the Zadoks growth scale, as described by Zadoks et al. (1974), leaf area and dry matter were measured in the Crop Physiology Laboratory, Department of Agronomy at Gorgan University of Agricultural Sciences and Natural Resources at each stage of sampling. The LAI was measured using the DELTA-T model leaf area meter, which adjusted by recorded plant density. The Kolmogorov-Smirnov test was used to check whether the variable distributions were normal using SAS statistical software (version 22.0).

CGR Calculation

The estimation of CGR in this study involves a comprehensive four-step process, as illustrated in Fig. 2. The CGR in grams per square meter per day (g m^{-2} day^{-1}) was calculated using the Eq. (1) (Sinclair, 1986):

$$CGR = SRAD \times 0.48 \times \left(a + b \times \frac{n}{N}\right) \times FINT \times RUE \quad (1)$$

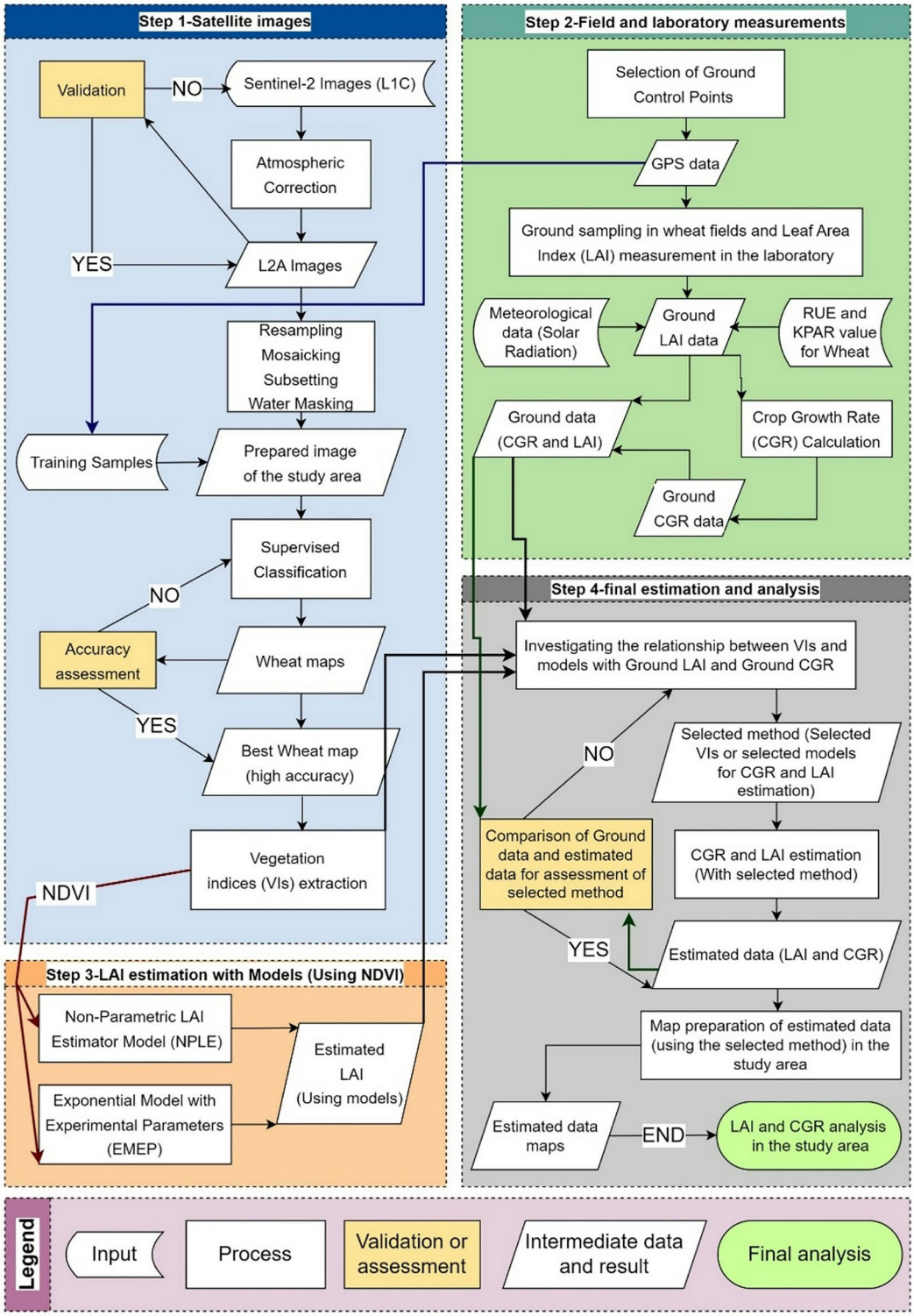

Fig. 2 A flowchart depicting the process of estimating Crop Growth Rate (CGR) in wheat fields. The legend clarifies the meaning of five different shapes used in the diagram. Step 1 (blue) and Step 2 (green) would run simultaneously. Then, Step 3 (orange) is run, resulting in Step 4 (gray), where the final analysis is conducted. This includes evaluating the Leaf Area Index (LAI) and analyzing CGR within the study area

Where SRAD, FINT, and RUE represent terrestrial solar radiation (MJ m^{-2} day^{-1}), the fraction of incident radiation intercepted by the leaves, and radiation use efficiency (g MJ^{-1}), respectively. The factor 0.48 is used to convert solar radiation (SRAD) to Photosynthetic Active Radiation (PAR) (Monteith & Unsworth, 2007). *a* and *b* are Ångström coefficients (typically equal to 0.25 and 0.5), *n* and *N* also denote sunshine hours and day length (hours), respectively (Ångström, 1924).

FINT was calculated using the Beer-Bouguer-Lambert Law (Eq. (2), Monteith, 1969), where KPAR represents the light extinction coefficient (Sinclair, 2006). The RUE for wheat was set at 2.2 g MJ^{-1}, and KPAR at 0.65, following the methodology proposed by Soltani and Sinclair (2012).

$$FINT = 1 - exp^{-KPAR\times\ LAI} \tag{2}$$

Satellite Data Source

In this study, 15 Sentinel-2 images were used, with three image frames for each date. These images, obtained at the L1C correction level, correspond to map part codes T40SCG, T40SBG, and T40SCF. They were acquired in sync with field sampling on specific dates in 2021: February 28, March 30, April 4, April 14, and May 9. All images were sourced from the Copernicus Open Access Hub (https://scihub.copernicus.eu/).

Pre-processing and Water Masking

Fifteen Sentinel-2 images (100 km × 100 km swath) georeferenced in the UTM/WGS84 spatial reference (Thales Alenia Space France, 2021) were used. To ensure uniform spatial resolution, all spectral bands were resampled to a 10-meter pixel size. Mosaicking was performed due to the use of three image frames, with both resampling and mosaicking conducted in SNAP 8.0.5. Water bodies were identified using NDVI < 0 in SNAP 8.0.5, and accuracy was validated with 100 reference points to ensure the reliability of the water masking process.

Wheat Field Mapping and Classification

Wheat fields were delineated by subsetting Sentinel-2 mosaicked images using predefined study area shapefiles. Pre-classification images were prepared for each sampling date, followed by supervised classification using ENVI 5.3. The classification method with the highest accuracy was selected for final mapping. Supervised classification, a widely used approach for land cover mapping (Jensen, 2015; Lu & Weng, 2007), was applied to classify wheat, canola, and residential/bare lands using Maximum Likelihood Classification (MLC), Minimum Distance to Means, and Mahalanobis Distance methods. Fifty training samples per class were used, while water bodies and forests were excluded through vegetation removal and water masking.

Classification accuracy was evaluated using an error matrix and Kappa coefficient (Cohen, 1960, Eq. (3)), categorizing agreement levels as strong (Kappa > 0.8), moderate (0.4 ≤ Kappa ≤ 0.8), or low (Kappa < 0.4) (Foody, 2002). A total of 300 reference points, selected via stratified random sampling, were used for validation. All analyses were performed in ENVI 5.3.

$$\text{Kappa Coefficient} = \frac{\text{Total Sample} \times \text{Total Correct Sample} - \sum (\text{Column. Total} \times \text{Row Total})}{(\text{Total Sample})^2 - \sum (\text{Column. Total} \times \text{Row Total})} \tag{3}$$

Wheat Field Mapping and Classification

A total of seven Vegetation Indices (VIs)—NDVI, DVI, RVI, IPVI, TVI, MSAVI, and SQRT(IR/R)—were computed and assessed (see Table 1) using SNAP software version 8.0.5. VIs are mathematical combinations of spectral bands, particularly in the red, green, and infrared wavelengths, designed to establish functional relationships between crop characteristics and remote sensing data (Wiegand et al., 1989).

Table 1 Spectral vegetation indices (VIs) analyzed in this study♣

Vegetation indices (VIs)	abbreviation	Equation	References
Difference Vegetation Index	DVI	b8-b4	Tucker, 1979
Normalized Difference Vegetation Index	NDVI	(b8-b4)/(b8+b4)	Rouse et al., 1974
Ratio Vegetation Index	RVI	b8/b4	Pearson & Miller, 1972
Infrared Percentage Vegetation Index	IPVI	b8/(b8+b4)	Crippen, 1990
Transformed Vegetation Index	TVI	$\sqrt{(b8-b4)/(b8+b4)+0.5}$	Rouse et al., 1974
Modified Soil Adjustment Vegetation Index	MSAVI	(1+L) (b8-b4)/(b8+b4+L)	Qi et al., 1994
SQRT(IR/R)	SQRT(IR/R)	$\sqrt{b8/b4}$	Tucker, 1979

♣In all formulas, b4 is the red band and b8 is the NIR band

Evaluation of Vegetation Indices (VIs)

After calculating the VIs, their numerical values were extracted at corresponding sampling locations, and the relationships between the VIs and ground data, including LAI and CGR, were analyzed. Pearson correlation coefficients (PCC) were also determined using SPSS (v.22.0).

Estimation of LAI Using NDVI-derived Empirical Models

In addition to the VIs derived from satellite imagery, two empirical models based on the Normalized Difference Vegetation Index (NDVI)—NPLE (Su, 1996) and EMEP (Viña et al., 2011)—were used to estimate LAI. These models were tested for significance using ground-based LAI data, and the model with the highest performance was selected for LAI estimation.

Nonparametric LAI Estimator Model (NPLE)

The NPLE model, was given by Eq. (4):

$$LAI = \sqrt{\frac{1+NDVI}{1-NDVI}} \times \mathrm{NDVI} \tag{4}$$

Within vegetation, the NPLE model produces output values from 0 to 10 based on NDVI values. Its structure makes it highly sensitive to changes in LAI, especially in areas with high NDVI. As a result, the NPLE model highlights LAI variations in densely vegetated regions (Su, 1996).

Exponential Model with Experimental Parameters (EMEP)

The EMEP model established a relationship between NDVI and LAI using natural logarithmic and exponential functions (Eq. (5), Viña et al., 2011):

$$\mathrm{LAI} = \frac{\ln\left(\frac{1}{1-\left(\frac{\mathrm{NDVI}-\mathrm{Y_0}}{\mathrm{a}}\right)}\right)}{\mathrm{b}} \tag{5}$$

Where, the parameters a, b, and $\mathrm{Y_0}$ are model calibration parameters. Although the model lacked direct biophysical interpretations, it showed good performance in estimating LAI for crops like corn and soybeans (Viña et al., 2011).

Various statistical metrics employed for comparing estimated data (Model Outcomes and Vegetation Indices) with ground data (LAI and CGR) Include:

- Coefficient of determination (R^2)

$$\mathrm{R}^2 = 1 - \frac{\sum_{\mathrm{i}=1}^{\mathrm{n}} \left(\widehat{\mathrm{X}}_\mathrm{i} - \mathrm{X}_\mathrm{i}\right)^2}{\sum_{\mathrm{i}=1}^{\mathrm{n}} \left(\mathrm{X}_\mathrm{i} - \bar{\mathrm{X}}_\mathrm{i}\right)^2} \tag{6}$$

- oot Mean Square error (RMSE).

$$\mathrm{RMSE} = \sqrt{\frac{\sum_{\mathrm{i}=1}^{\mathrm{n}} \left(\hat{X}_\mathrm{i} - \mathrm{X}_\mathrm{i}\right)^2}{\mathrm{n}}} \tag{7}$$

- Mean Absolute Error (MAE).

$$\mathrm{MAE} = \frac{1}{\mathrm{n}} \times \sum_{\mathrm{i}=1}^{\mathrm{n}} \left|\widehat{X}_\mathrm{i} - \mathrm{X}_\mathrm{i}\right| \tag{8}$$

- Mean Bias Error (MBE).

$$\mathrm{MBE} = \frac{1}{\mathrm{n}} \times \sum_{\mathrm{i}=1}^{\mathrm{n}} \left(\widehat{X}_\mathrm{i} - \mathrm{X}_\mathrm{i}\right) \tag{9}$$

In these equations, $\widehat{X}_\mathrm{i}$and $\mathrm{X_i}$ represent the estimated and measured values (LAI and CGR), respectively, " $\bar{\mathrm{X}}_\mathrm{i}$" is the mean of all measured values, and *n* is the number of observations. High estimation accuracy was indicated by the highest R^2 values, the lowest RMSE and MAE values, and MBE values closest to zero (with negative MBE indicating underestimation and positive MBE indicating overestimation).

After evaluating each method using these criteria, the most accurate vegetation index (VI) or model was selected to compute LAI and CGR values. These values were then mapped using ArcGIS version 10.6.1 based on the derived mathematical equations.

Although this study did not focus on water consumption and crop yield, the prominent physiological indices of LAI, CGR, and NAR are strongly linked to these traits in agroecosystems. LAI affects absorbed radiation and transpiration in canopies, which, in turn, affects evapotranspiration and water use efficiency. CGR also serves as an important component for yield potential, especially when water supply is variable. NAR, which represents photosynthetic efficiency per unit leaf area, is critical for effective dry matter partitioning to reproductive sinks. Mapping and comparing these indices in a study area provides indirect insights into spatial variability in resource use and productivity in agroecosystems, serving as a physiological basis for future integration with crop yield and water-use data to support yield gap assessments.

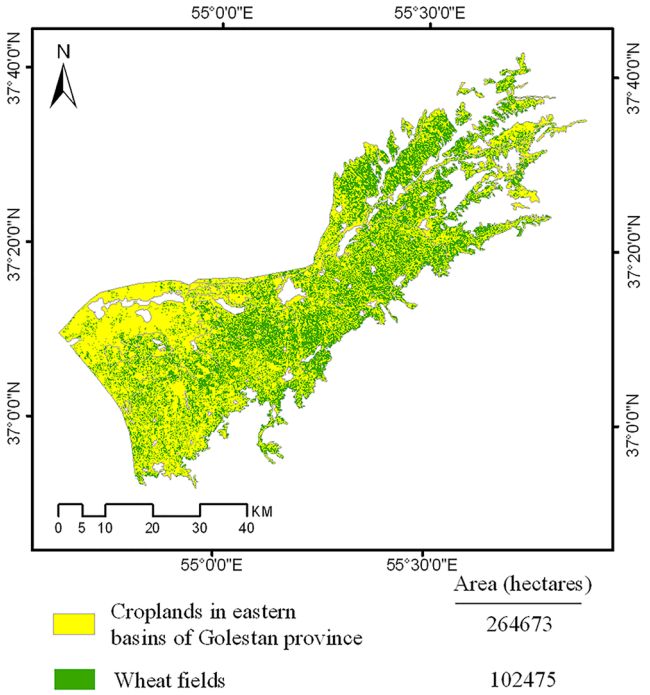

Fig. 3 Map of Wheat-cultivated fields in Eastern Basins, Golestan Province, Iran, utilizing Sentinel-2 Imagery and the Maximum Likelihood Classification (MLC) method

Results and Discussion

Water Masking and Wheat-Grown Fields Detection Accuracy

The water masking using negative NDVI values (NDVI < 0) effectively identified and masked all 100 reference points corresponding to water bodies. This simple and reliable approach could be a valuable method for distinguishing water cover in cropland studies. The accuracy of wheat-grown fields detection was also assessed using multiple supervised classification methods and reference points. Among these methods, Maximum Likelihood Classification (MLC) achieved the highest precision, with a Kappa coefficient (K) of 0.96 for the March 30 image (data not shown). The effectiveness of the MLC has been reported by other researchers (Hussain et al., 2022; Rahimi-Ajdadi, 2022; Seyam et al., 2023).The map of detected wheat-cultivated fields in the study area are presented in Fig. 3.

Evaluation of Vegetation Indices (VIs) for LAI and CGR Estimation Across Phenological Stages

The evaluation of vegetation indices (VIs) derived from Sentinel-2 imagery and their correlation with ground-based measurements of LAI and CGR across different wheat phenological stages demonstrated significant variability in performance. MSAVI, DVI, and SQRT(IR/R) consistently exhibited strong correlations across all development stages, making them reliable indicators for monitoring wheat LAI and CGR. Notably, the SQRT(IR/R) index showed the highest correlation in two of the five LAI comparison stages. Originally introduced by Tucker (1979) and structurally expressed as SQRT(RVI), this index is closely related to RVI, which was developed by Pearson and Miller (1972) and is widely used in LAI studies. Correlation strength varied by phenological stage, with the highest values observed during early (stem elongation) and late (milk development) development stages, while weaker relationships were recorded during middle reproductive phases (middle ear emergence and flowering).

Table 2 highlights the detailed Pearson correlation coefficients (PCC) comparing VIs with LAI and CGR across five key wheat development stages. During stem elongation, all Vis ($p < 0.01$) showed strong positive correlations with LAI (PCC > 0.85) and CGR (PCC > 0.84), with SQRT(IR/R) (PCC = 0.937) and RVI (PCC = 0.934) demonstrating the highest correlation with LAI. Middle ear emergence presented more variability in correlation strength, with DVI

Table 2 Pearson correlation coefficients (PCC) analysis comparing vegetation indices derived from Sentinel-2 images with ground-based measurements of LAI and CGR at five key wheat development stages in the research area

Images	Variable-developmental stage	Vegetation indices (VIs)						
		MSAVI	IPVI	SQRT(IR/R)	DVI	TVI	NDVI	RVI
Feb 28	LAI (stem elongation)	**0.917	**0.899	**0.937	**0.858	**0.895	**0.899	**0.934
	CGR (stem elongation)	**0.910	**0.920	**0.913	**0.845	**0.918	**0.920	**0.891
Mar 30	LAI (middle ear emergence)	**0.718	*0.339	*0.358	**0.770	*0.338	*0.339	**0.382
	CGR (middle ear emergence)	**0.507	0.176 $^{n.s}$	0.172 $^{n.s}$	**0.561	0.175 $^{n.s}$	0.176 $^{n.s}$	0.214 $^{n.s}$
Apr 4	LAI (late ear emergence)	**0.800	**0.613	**0.617	**0.802	**0.612	**0.613	**0.618
	CGR (late ear emergence)	**0.758	**0.608	**0.607	**0.755	**0.608	**0.608	**0.606
Apr 14	LAI (Flowering)	**0.924	**0.830	**0.832	**0.919	**0.829	**0.830	**0.827
	CGR (Flowering)	**0.451	**0.388	**0.455	**0.441	**0.384	**0.388	**0.477
May 9	LAI (milk development)	**0.952	**0.951	**0.961	**0.943	**0.946	**0.951	**0.947
	CGR (milk development)	**0.927	**0.962	**0.929	**0.913	**0.963	**0.962	**0.897

**Significant at the 0.01 level; * Significant at the 0.05 level; n.s. Not significant

(PCC = 0.561, $P < 0.01$) and SQRT(IR/R) (PCC = 0.507, $p < 0.01$) maintaining significant relationships, while NDVI and TVI exhibited non-significant correlations. Correlations recovered during late ear emergence and flowering, with CGR reaching exceptionally high values (PCC > 0.94, $p < 0.01$) during the flowering stage, indicating that VIs may be more reliable for growth rate estimation than canopy structure during this phase. The milk development stage recorded the highest correlations with LAI, with NDVI and TVI achieving near-perfect correlations (PCC = 0.962 and 0.963, $p < 0.01$, respectively), confirming their suitability for late-stage LAI estimation. Among the indices, DVI and SQRT(IR/R) were the most effective for LAI estimation, while MSAVI and SQRT(IR/R) performed best for CGR.

Evaluation of Vegetation Indices (VIs) for LAI and CGR Estimation Across Phenological Stages

The performance evaluation of the NPLE and EMEP models for estimating both Leaf Area Index (LAI) and Crop Growth Rate (CGR) across different phenological stages demonstrated satisfactory outcomes, with notable differences in accuracy at various growth stages (Figs. 4 and 5).A, B and Y0 coefficients for EMEP model were adjusted and calibrated as 0.7298, 0.2064 and 0.6159, respectively. Both models performed well at later development stages, particularly during milk development, where R^2 values reached 0.923 ($p < 0.01$) for NPLE and 0.926 ($p < 0.01$) for EMEP in LAI estimation, with low RMSE values of 0.216 and 0.313, respectively. Similar trends were observed for CGR, where both models captured growth dynamics accurately during later phenological stages, reflecting their robustness at these critical phases.

However, during earlier development stages (middle ear emergence and late ear emergence), the models exhibited reduced accuracy, with lower non-significant R^2 values (0.138–0.38) and higher error metrics for both LAI and CGR, likely due to greater variability in canopy structure and environmental factors. Despite these challenges, EMEP generally outperformed NPLE, particularly in CGR estimation, with consistently lower mean bias error (MBE) and root mean square error (RMSE) values across most development stages. This suggests that EMEP has a slight edge in capturing growth rate dynamics in wheat fields, especially during periods of rapid growth. These results emphasize the importance of selecting appropriate VIs based on

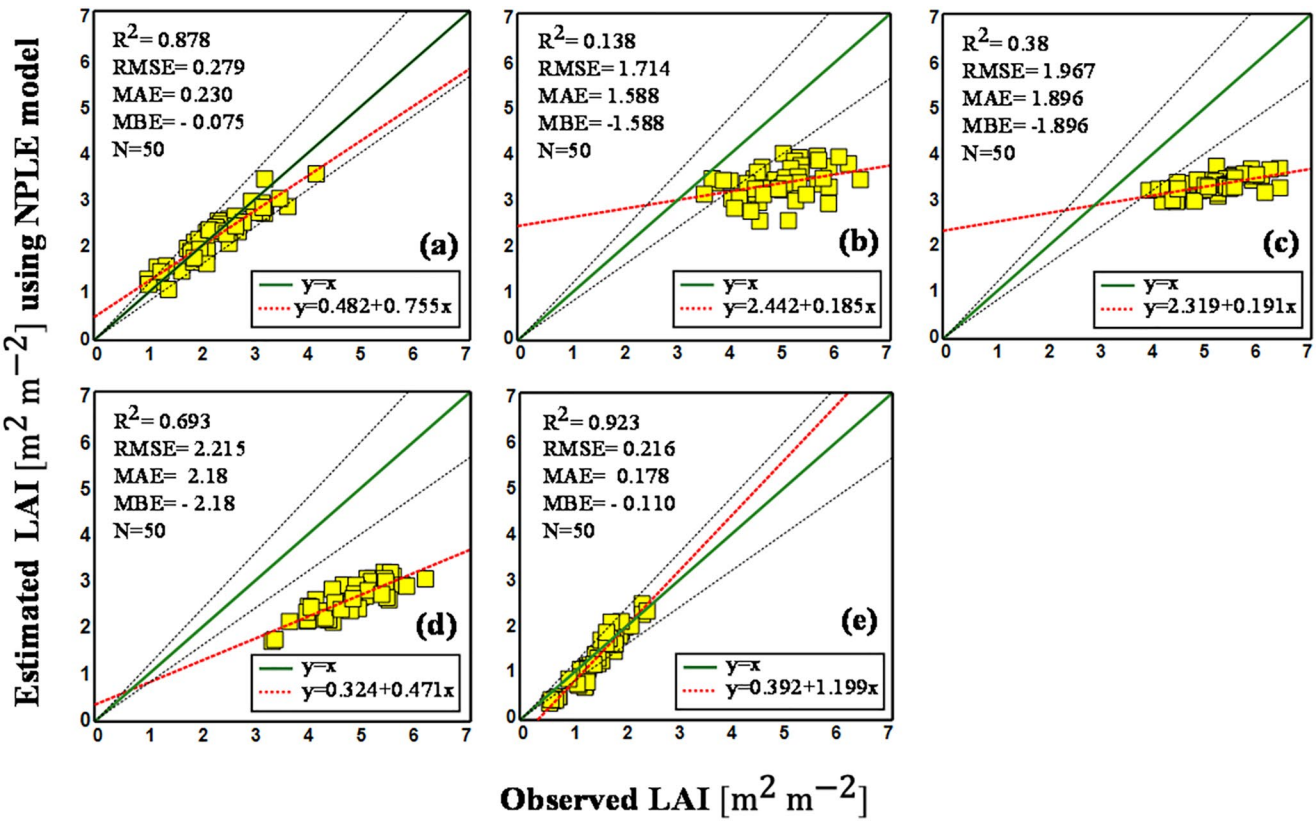

Fig. 4 Scatterplots comparing observed LAI (field measurements) with LAI estimates generated by the NPLE model across various wheat phenological stages: (**a**) stem elongation, (**b**) middle ear emergence, (**c**) late ear emergence, (**d**) flowering, and (**e**) milk development. The green dashed line represents the 1:1 agreement line, while the red dashed line illustrates the linear regression fitting line, highlighting the relationship between the observed and estimated data

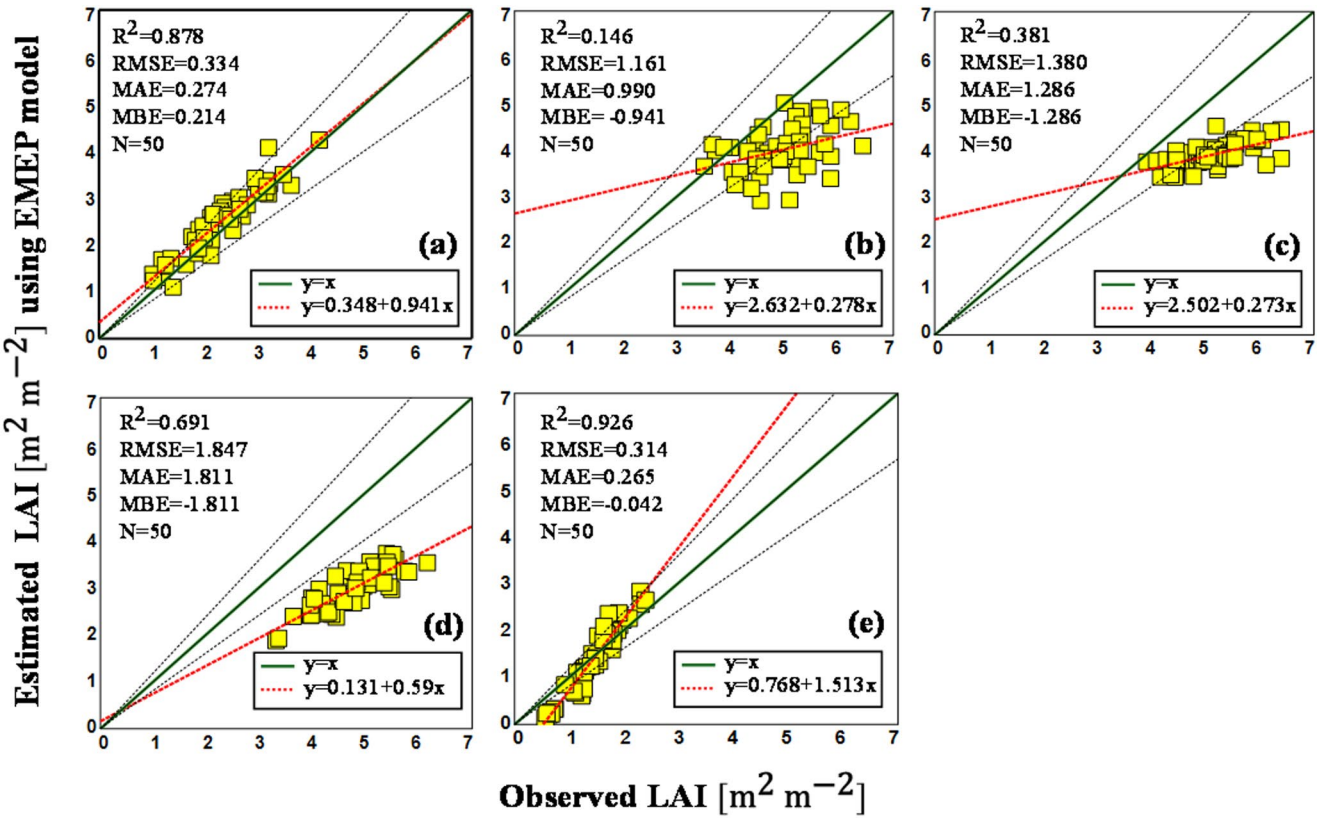

Fig. 5 Scatterplots comparing observed LAI (field measurements) with LAI estimates generated by the EMEP model across various wheat phenological stages: (**a**) stem elongation, (**b**) middle ear emergence, (**c**) late ear emergence, (**d**) flowering, and (**e**) milk development. The green dashed line indicates the 1:1 agreement line, while the red dashed line represents the linear regression fitting line, highlighting the relationship between the observed and estimated data

Table 3 Selected vegetation indices (VIs) for accurate Estimation of leaf area index (LAI) and crop Groeth rate (CGR) at five critical wheat phenological stages

Selected Vis		
Phenological stage/sampling	Leaf area index (LAI)	Crop growth rate (CGR)
Stem elongation	SQRT(IR/R)	IPVI
middle ear emergence	DVI	DVI
late ear emergence	DVI	MSAVI
Flowering	MSAVI	RVI
milk development	SQRT(IR/R)	TVI

development stage to enhance Sentinel-2-based crop monitoring accuracy. Integrating multiple indices, particularly MSAVI, DVI, and SQRT(IR/R), could further improve the precision of remote sensing applications in wheat growth assessment.

Comparison Between VIs and Empirical Models

In this study, vegetation indices (VIs) were selected over more complex empirical models due to their strong correlation with ground-based measurements such as LAI and CGR. As shown in Table 2, Pearson correlation coefficients (PCC) between VIs derived from Sentinel-2 imagery and ground-based data consistently demonstrated significant relationships across various wheat development stages, highlighting their reliability for predicting vegetation state. While empirical models provide robust and accurate estimates, particularly in late development stages, VIs offer greater flexibility and real-time adaptability. Compared to empirical models, VIs are cost-effective, provide timely and repeatable data, and can be applied on a large scale, making them highly suitable for operational agricultural monitoring. Therefore, given their high correlation with key biophysical parameters, VIs were prioritized (as Table 3) for further analysis to streamline vegetation assessment while preserving accuracy. Observed versus predicted values for LAI and CGR using different VIs as dependent variables, along with associated statistical metrics, are presented in Figs. 6 and 7, respectively.

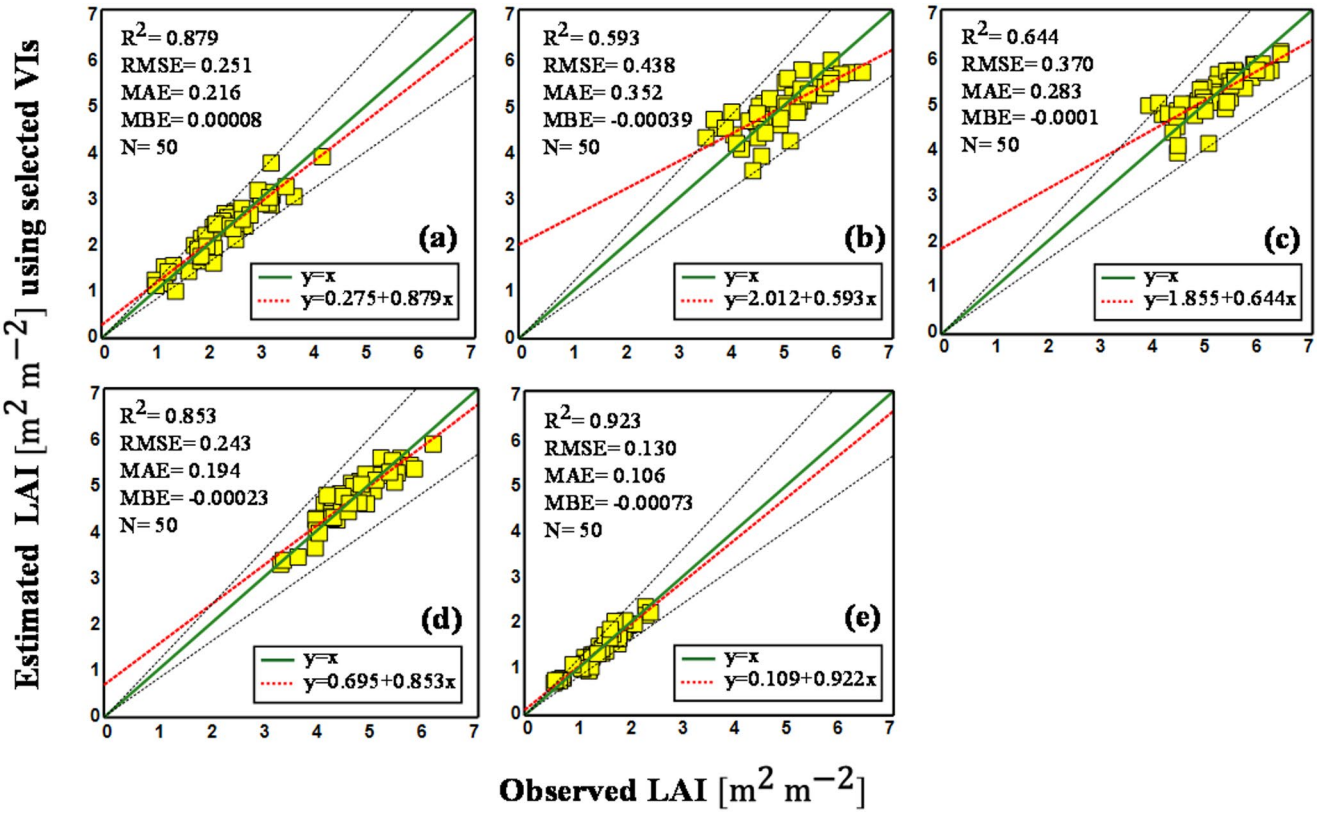

Fig. 6 Scatterplots comparing field-measured LAI with estimated LAI using selected vegetation indices (VIs) across different wheat development stages: (**a**) stem elongation with SQRT(IR/R), (**b**) middle ear emergence with DVI, (**c**) late ear emergence with DVI, (**d**) flowering with MSAVI, and (**e**) milk development with SQRT(IR/R). Each scatterplot features a green dashed line indicating the 1:1 agreement line and a red dashed line representing the linear regression fit, highlighting the relationship between the data points

Spatial-Temporal Maps of LAI and CGR in Wheat Fields of Eastern Watershed Basins of Golestan Province: Implications for Crop Management

The LAI estimated maps for wheat-cultivated fields in eastern watershed basins of Golestan Province, as depicted in Fig. 8, illustrate the spatial distribution and temporal changes of LAI across different phenological stages. The minimum and maximum LAI values observed in the study area varied significantly with the progression of wheat development stages. During the stem elongation stage, the LAI exhibited its initial increase, with values ranging from a minimum of approximately 2.5 to a maximum of 4.5 (for the major parts of wheat fields), indicating the early development of leaf biomass. In the middle ear emergence stage, LAI values increased further, reflecting enhanced canopy density and vigor, with minimum and maximum values shifting to 3 and 5.5 (for major parts), respectively. The trend continued into the late ear emergence stage, where LAI peaked in certain areas, showing values between 2.97 and 6.88. Mohammadi et al. (2015) stated that the wheat LAI in Golestan Province ranged from 0.304 to 2.317 and from 2.66 to 6.049 in the tillering and booting stages, respectively. Considering the maximum obtainable LAI and the significant variation between fields (while the majority of fields show a maximum LAI of 4 to 5.5) shows that the potential of arable lands and the management level in the fields cause the gap between the maximum expected LAI and the actual obtained LAI, although positive feedback between LAI and fraction of absorbed radiation could not be ignored. The observed peak LAI during the late ear emergence stage corresponds with the crop's maximum vegetative growth, which is critical for assimilate accumulation. The subsequent decline in LAI during the flowering and milk development stages can be attributed to leaf senescence and the plant's shift in resource allocation from vegetative growth to grain filling. Eyni-Nargeseh et al. (2020) reported that the reduction in CGR is attributed to leaf senescence during the post-flowering stage and the allocation of a greater proportion of photosynthetic assimilates to the grains. These variations in LAI provide valuable information for optimizing agricultural practices. CGR also peaked at the late ear emergence stage, with spatial and temporal variations during different phenological stages (Fig. 9). The peak CGR during the late ear emergence stage signifies the period of maximum photosynthetic efficiency and nutrient assimilation, critical

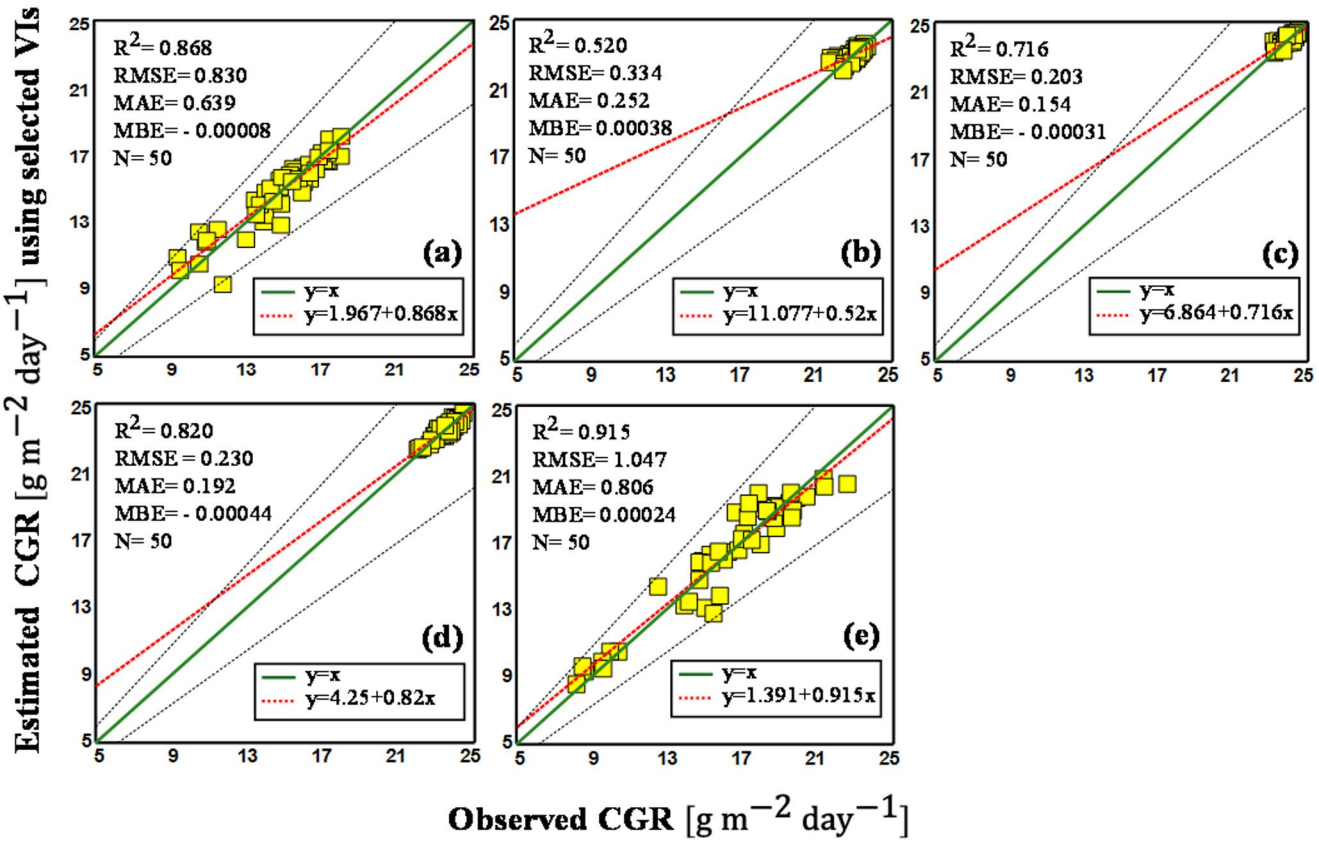

Fig. 7 Scatterplots illustrating the comparison between field-measured CGR and computationally estimated CGR using selected vegetation indices (VIs) across different wheat development stages: (**a**) stem elongation with IPVI, (**b**) middle ear emergence with DVI, (**c**) late ear emergence with MSAVI, (**d**) flowering with RVI, and (**e**) milk development with TVI. The green dashed lines indicate the 1:1 agreement line, while the red dashed lines represent linear regression fitting lines, highlighting the relationships within the data

for determining final yield potential. The gradual decline in CGR observed during the flowering and milk development stages can be attributed to the shift in the plant's physiological priorities from vegetative expansion to reproductive development and grain filling. The maximum CGR at the late ear emergence stage varied from 20.66 to 24.73 gr m^{-2} day^{-1} (Fig. 10), which is far below the maximum reported CGR for C3 plants, as stated by Monteith (1978), where the maximum growth rate for C3 stands falls in the range of 34–39 gr m^{-2} day^{-1}.

The findings show that the major parts of the wheat fields in the study area have moderate LAI (3 to 5.5) and CGR (22–24.73 gr m^{-2} day^{-1}) at the late ear emergence stage, highlighting the necessity of managing wheat-grown fields to optimize CGR.

Temporal Trends of LAI, CGR and NAR in Wheat Fields of Eastern Watershed Basins of Golestan Province Across the Growing Season

As expected, we observed a strong synchrony between CGR and LAI trends (Fig. 11A&B), with their peaks coinciding during the late ear emergence stage, while NAR values are not significantly different in all watershed basins (Fig. 11C). The results clearly show that CGR values align with LAI changes across different phenological stages, while NAR remains relatively stable in all watershed basins. This reveals that LAI is the prominent trait driving CGR values compared to NAR. Since CGR is a product of LAI and NAR, and NAR is relatively stable in all watershed basins, our results demonstrate that LAI has a more pronounced effect on CGR. This highlights the importance of canopy development and leaf area expansion (as reflected in LAI) in influencing biomass accumulation during the late ear emergence stage.

It's worth highlighting that the values of LAI (and CGR) exhibit significant variability across different watershed basins, indicating that they are influenced by various factors, especially during the transition from middle ear emergence to flowering phenological stages. These findings suggest that leaf senescence initiates before the onset of flowering in wheat-cultivated fields in the study area, resulting in a short period of maximum LAI. Consequently, the wheat fields in our study area do not achieve the anticipated maximum

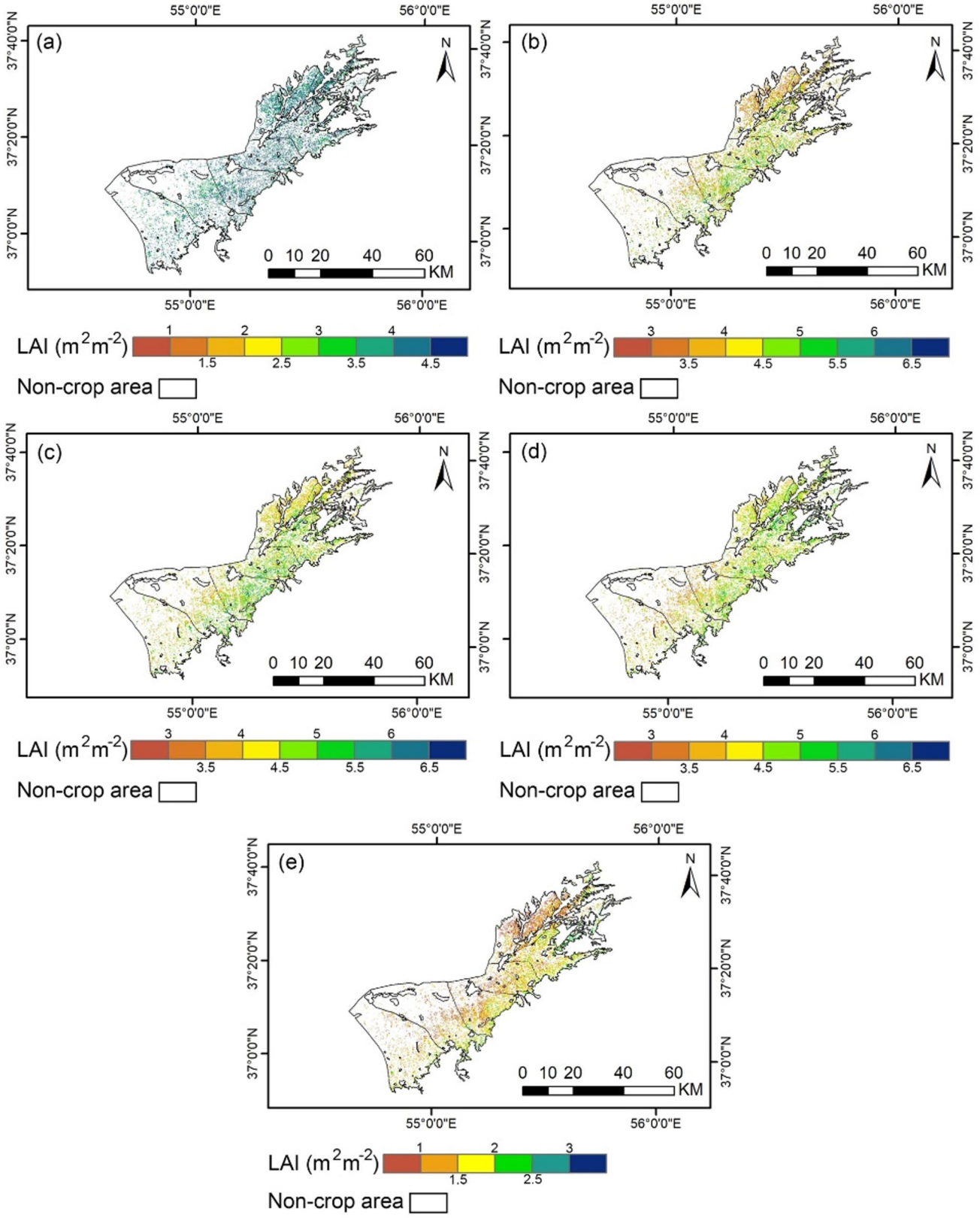

Fig. 8 LAI estimation maps for wheat fields in eastern Golestan Province's croplands using selected VIs at the phenological stages included (**a**) stem elongation using SQRT(IR/R), (**b**) middle ear emergence using DVI, (**c**) late ear emergence using DVI, (**d**) flowering using MSAVI, and (**e**) milk development using SQRT(IR/R)

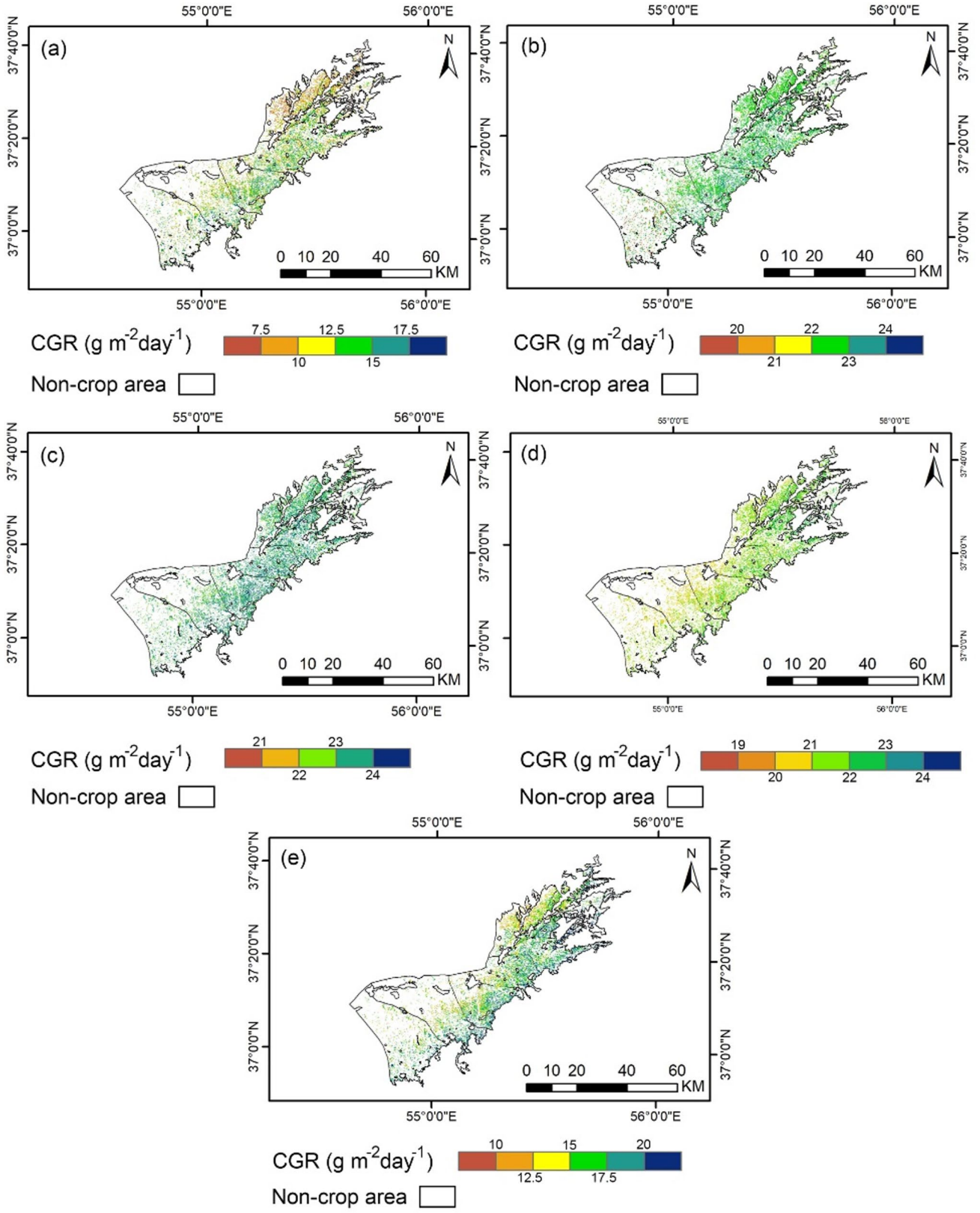

Fig. 9 Crop growth rate (CGR) maps for wheat fields in the croplands of Golestan Province's eastern basins using specific vegetation indices (VIs) during various phenological stages: (**a**) stem elongation with IPVI, (**b**) middle ear emergence with DVI, (**c**) late ear emergence with MSAVI, (**d**) flowering with RVI, and (**e**) milk development with TVI

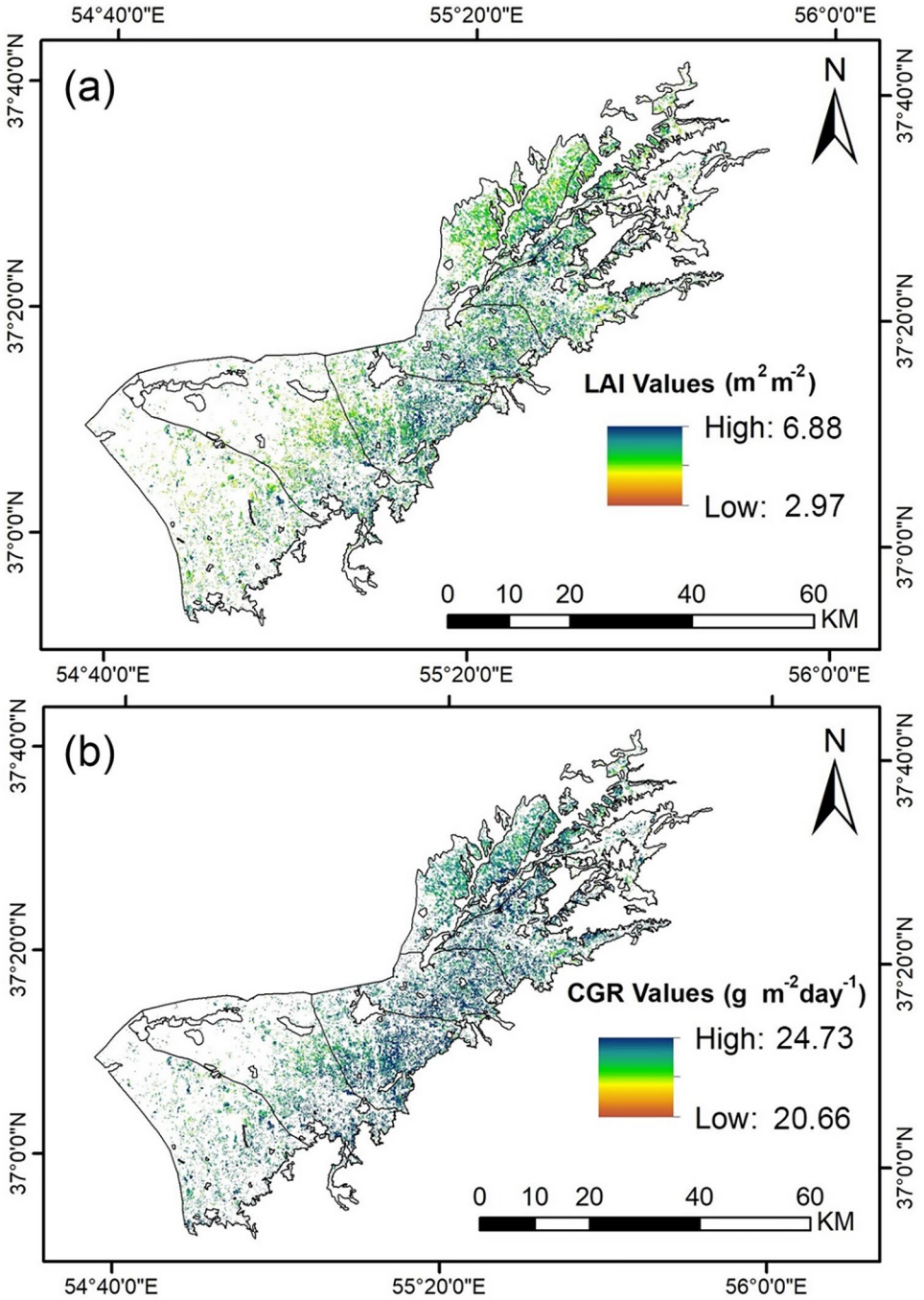

Fig. 10 The estimated Crop Growth Rate (CGR) values and estimated Leaf Area Index (LAI) values at late ear emergence, as part of the LAI and CGR analysis within the study region, encompassing wheat fields in the croplands of the eastern basins of Golestan Province. Notably, this stage exhibited the highest estimated values for both LAI and CGR

CGR for wheat cultivars, with the highest observed value being 24 g m^{-2} day^{-1}. The synchrony of the middle phenological stages of wheat with frequently cloudy days in February to March, a pattern associated with the Caspian Sea's proximity, contributes to a sharp decline in both LAI and CGR after the late ear emergence stage, alongside other physiological factors like nitrogen remobilization. Considering these results, it is prudent to explore strategies aimed at increasing the fraction of absorbed radiation, which could hold promise for future breeding programs.

Crop Growth Rate (CGR) is a key indicator of wheat productivity, influenced by various factors including temperature (Kuroyanagi, 1985), soil quality, organic fertilizers (Hossain et al., 2021), and nutrient sources (Khan et al., 2017), which are optimal in input-intensive wheat-cultivated fields in Golestan Province with suitable climatic conditions for wheat production (except for radiation). Our study showed the CGR and LAI peak values of 24.73 g m^{-2} d^{-1} and 6.88 for wheat-cultivated fields, respectively, which

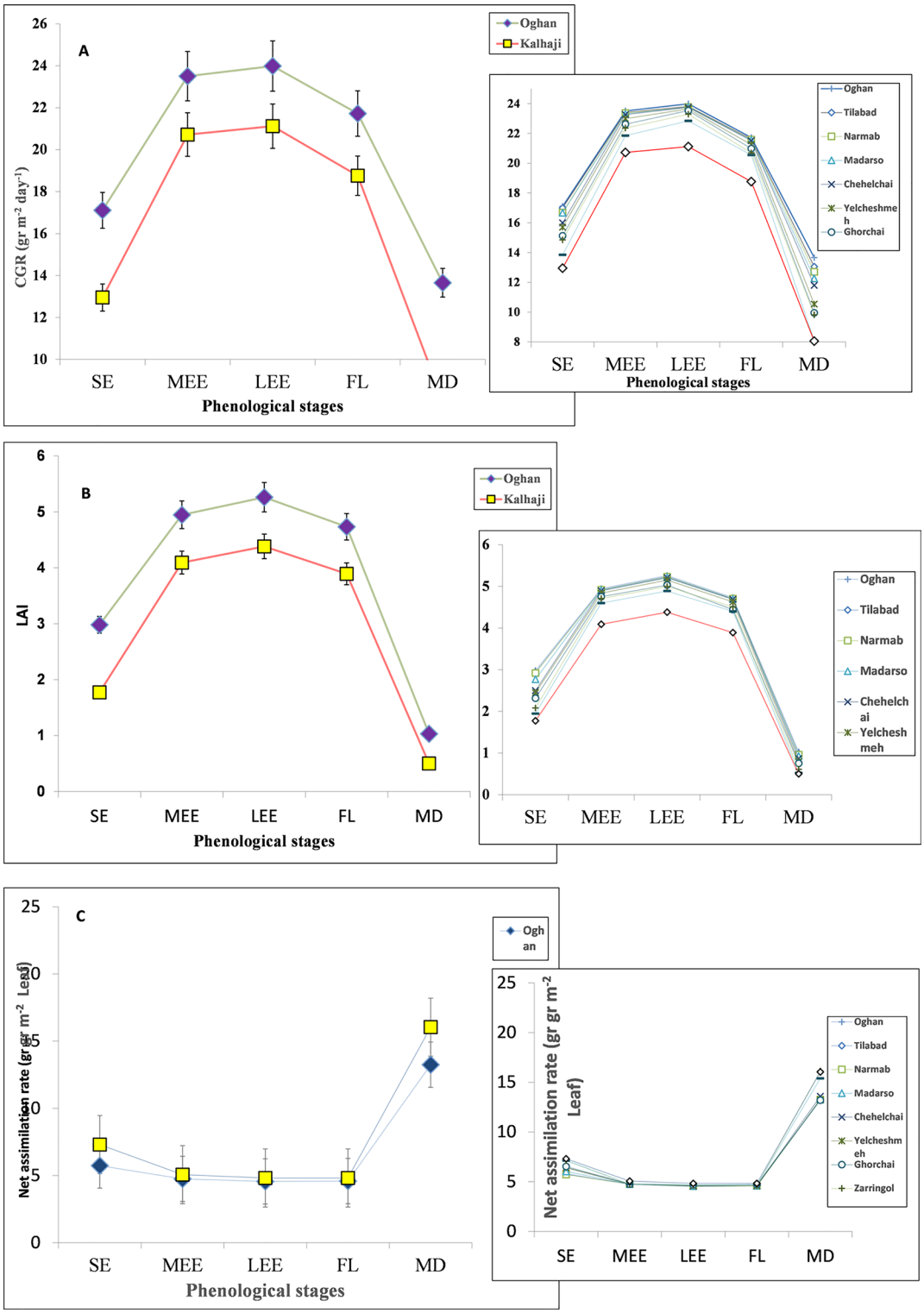

Fig. 11 Trends of (**A**) Crop Growth Rate (CGR), (**B**) Leaf Area Index (LAI) and (**C**) Net Assimilation Rate (NAR) across five phenological stages (SE: Stem elongation, MEE: middle ear emergence, LEE: late ear emergence, FL: flowering, MD: milk development) in study area watersheds. The larger left panels for each trait display the watershed basins with the highest and lowest values, while the smaller right panels show the values across all watershed basins

is less than the potential (peak) of CGR reported by Monteith (1978) (34–39 g m^{-2} d^{-1}).

Many studies in the Golestan Province on crops such as canola (Faraji, 2012; Biabani et al., 2021), cotton (Saberpour et al., 2022), and winter cereals (Rahemi-Karizaki et al., 2021) further support the interplay between LAI, radiation interception, and CGR. Solar radiation (SRAD) is particularly crucial for biomass accumulation and yield (Gurjar et al., 2017). However, in Golestan Province, persistent cloud cover during grain filling leads to reduced SRAD, limiting CGR and yield potential. This aligns with findings by Eyni-Nargeseh et al. (2020), who emphasized the importance of early-stage CGR through efficient light absorption via expanded leaf area. The different LAI production could be a main source for different CGR of studied fields in different watershed basins, along with low incident radiation from February to March in all watershed basins, which explains why the observed CGR is lower than the expected maximum. Maximizing wheat yield in low-SRAD regions like Golestan requires optimizing radiation interception, which is directly related to LAI. Rahemi-Karizaki et al. (2021) highlighted the impact of LAI dynamics on dry matter accumulation, underscoring the need to align crop phenology with seasonal radiation patterns. Ensuring crops reach and maintain maximum LAI during peak radiation periods is vital. This can be achieved by selecting cultivars with rapid leaf expansion, prolonged Leaf Area Duration (LAD), and improved canopy structure. Sowing date optimization also enhances SRAD capture. Further yield improvements hinge on increasing Radiation Use Efficiency (RUE) and optimizing canopy structure. While NAR was stable in all watershed basins, using cultivars with higher light absorption fractions or enhanced RUE is well-suited for the studied area. Yunusa et al. (1993) observed higher light extinction coefficient (K) values and RUE in modern wheat cultivars, a finding echoed by Tao et al. (2018). Given that modern varieties already approach the theoretical Harvest Index (HI) limit (Acreche et al., 2009; Li et al., 2022), future yield gains will depend more on radiation capture and conversion efficiency (Furbank et al., 2015; Xiao et al., 2020; Wang et al., 2019). Therefore, a shift from HI-centric strategies to those emphasizing light interception and RUE is warranted. This includes breeding for optimal phenological traits, ideal canopy architecture (e.g., leaf angle adjustment), and appropriate plant densities. Agricultural extension services and breeding programs must collaborate to disseminate and implement these strategies effectively.

Conclusion

Monitoring the LAI and CGR during five critical phenological stages revealed that he critical stages where the LAI and CGR in the studied watershed basins begin to diverge occur after the late ear emergence stage. During this stage, both LAI and CGR parameters typically experience their peak values, indicating maximum canopy cover (high LAI and canopy closure) and rapid biomass accumulation (represented by high CGR). However, as the crop shifts into flowering and milk development stages, LAI and CGR start to decrease. At flowering stage, LAI remains relatively stable or slightly declines as the canopy reaches full maturity, while CGR begins to decrease more sharply due to slower biomass accumulation. This divergence marks the shift in the plant's focus from vegetative growth to reproductive development. In the milk development stage, the divergence becomes more pronounced. LAI declines as leaves begin to senesce, whereas CGR drops significantly because the crop's energy is redirected toward grain filling rather than producing new biomass. This stage represents the final transition from active growth to the maturation phase. Understanding these stages is crucial for targeted management practices, as it helps farmers focus on sustaining canopy health and optimizing resource use during early growth while ensuring enough energy is available for reproductive success in later stages.

Our study showed although satellite imagery could help us to analyze and interpret the state of agroecosystems, but precise determination of the satellite imagery-based indices or products is necessary for up-scaling the single-vitiate relationships to the whole study area. After setting and testing the accuracy of the equations, trend analysis of physiological parameters in the agroecosystems would be possible. Time-series mapping of CGR, LAI and NAR helped us to find LAI optimization is most prominent and promising trait that can fill the gap of CGR between wheat-cultivated lands in different watershed basins. Our results on NAR revealed that photosynthetic performance per unit leaf area in all wheat cultivars is relatively consistent, and differences in crop growth are likely due to LAI or other structural traits. Optimizing the LAI by strategic plans like appropriate sowing date, selecting cultivars with rapid leaf expansion, prolonged Leaf Area Duration (LAD), and improved canopy structure could improve fraction of absorbed radiation, especially in cloudy days of February to March (which contributes to a sharp decline in both LAI and CGR after the late ear emergence stage). Sensitivity analysis using process-oriented crop simulation models can help researchers identify the most suitable sowing dates, cultivars, and canopy structures to optimize the fraction of absorbed

radiation, thereby improving crop growth rate (CGR) and ultimately enhancing wheat yield in the study area.

Several considerations could be claimed in this study. Sensitivity of the empirical models used to local agro-climatic conditions and sensor noise could affect generalizability and upscaling of the results. Reliance on one growing season, which ignores year-to-year climatic variability and interannual trends, along with the lack of cultivar-specific physiological calibration (which affects NAR precision), also could be a source of errors in absolute values. However, these errors could be ignored when the outputs are used for comparing the trend of studied traits in different watershed basins during different crucial phenological stages.

Validating the models using cultivar-level physiological parameters, incorporating remote sensing-based procedures and process-oriented crop simulation models to refine a more robust sowing window, optimize canopy structure, and sustain Leaf Area Duration (LAD)—especially in the canopy closure stage—and expanding this framework for quantifying the effects of climate change using CMIP6 models to offer valuable solutions for adaptive crop management and regional food security planning are further research directions that could be recommended.

Acknowledgements We gratefully acknowledge the support of Gorgan University of Agricultural Sciences and Natural Resources for R. Akbari's thesis support. We also thank Mrs. Mina Farajzadeh for her kind help to redraw figures and flowcharts. We would also like to express our gratitude to Mrs. Mina Farajzadeh for her generous assistance in redrawing the figures and flowcharts.

Author Contributions Behnam Kamkar played a pivotal role in conceptualizing and designing the study as MT. Roohollah Akbari's dissertation supervisor, involving methodology, software training, and project administration. MT. Roohollah Akbari conducted farm surveys, gathered crucial data, curated information, and authored the initial draft. Dr. Parisa Alizadeh Dehkordi and Dr. Hossein Kazemi, acting as co-advisors to MT. Roohollah Akbari, contributed additional experimental data and offered input during draft reviews and revisions. Prof. Behnam Kamkar oversaw the final editing of the manuscript, ensuring its comprehensive finalization.

Funding This research did not receive any specific grant from funding agencies in the public, commercial, or not-for-profit sectors. We also thank the Gorgan University of Agricultural Sciences and Natural Resources University for its financial support in implementing Roohollah Akbari M.SC dissertation.

Data Availability The datasets generated and analysed during the current study are available from the corresponding author upon reasonable request.

Declarations

Declaration of competing interests – editorial board member As a member of the Editorial Board of the journal, I declare that I am fully committed to upholding the integrity of the peer review process. I understand and accept that I must exclude myself from handling any manuscripts where a competing interest exists. This includes, but is not limited to, cases where I have previously published with one or more of the authors, share the same institutional affiliation, or have any professional or personal relationships that may be perceived as a conflict of interest. Should I be listed as an author on a manuscript submitted to the journal, I will ensure that this is transparently declared in the "Competing Interests" section of the manuscript. I also acknowledge that such submissions will follow the journal's standard peer review process and will not be given any preferential treatment due to my Editorial Board position.In addition to financial interests, I am aware of the importance of disclosing any non-financial interests that may influence my editorial responsibilities, such as professional affiliations, advisory roles, or personal relationships. I commit to maintaining transparency and fairness in all aspects of my editorial duties.

Competing Interests The authors declare no financial or non-financial interests that could be perceived as directly or indirectly related to the work submitted.

References

Acreche, M. M., Briceño-Félix, G., Sánchez, J. A. M., & Slafer, A. G. (2009). Radiation interception and use efficiency as affected by breeding in mediterranean wheat. *Field Crops Research*, *110*(1), 91–97. https://doi.org/10.1016/j.fcr.2008.07.005

Ångström, A. (1924). Solar and terrestrial radiation. *Quarterly Journal of the Royal Meteorological Society*, *50*(210), 121–126. https://doi.org/10.1002/qj.49705021008

Biabani, A., Foroughi, A., Karizaki, A. R., Rassam, G. A., Hashemi, M., & Afshar, R. K. (2021). Physiological traits, yield, and yield components relationship in winter and spring Canola. *Journal of the Science of Food and Agriculture*, *101*(8), 3518–3528. https://doi.org/10.1002/jsfa.11094

Cohen, J. (1960). A coefficient of agreement for nominal scales. *Educational and Psychological Measurement*, *20*(1), 37–46.

Crippen, R. E. (1990). Calculating the vegetation index faster. *Remote Sensing of Environment*, *34*(1), 71–73. https://doi.org/10.1016/0034-4257(90)90085-Z

Eyni-Nargeseh, H., Deihimfard, R., Rahimi-Moghaddam, S., & Mokhtassi-Bidgoli, A. (2020). Analysis of growth functions that can increase irrigated wheat yield under climate change. *Meteorological Applications*, *27*(1), e1804. https://doi.org/10.1002/met.1804

FAOSTAT (2023). *Statistical database*. Food and Agriculture Organization of the United Nations. https://www.fao.org/faostat

Faraji, A. (2012). Flower formation and pod/flower ratio in Canola (*Brassica Napus* L.) affected by assimilated supply around flowering. *International Journal of Plant Production*, *4*(3), 271–280. https://doi.org/10.22069/ijpp.2012.710

Foody, G. M. (2002). Status of land cover classification accuracy assessment. *Remote Sensing of Environment*, *80*(1), 185–201.

Foresight. (2011). *The future of food and farming: Final project report*. The Government Office for Science.

Furbank, R. T., Quick, W. P., & Sirault, X. R. R. (2015). Improving photosynthesis and yield potential in cereal crops by targeted genetic manipulation: Prospects, progress, and challenges. *Field Crops Research*, *182*, 19–29. https://doi.org/10.1016/j.fcr.2015.04.009

Gurjar, G. N., Swami, S., Meena, N. K., & Lyngdoh, E. A. S. (2017). Effect of solar radiation in crop production. In S. Arora, S. Swami, & S. Bhan (Eds.), *Natural resource management for climate-smart sustainable agriculture* (pp. 103–115). Soil Conservation Society of India.

Hossain, M. A., Hasan, M. M., Hossain, M. B., & Islam, S. M. S. (2021). Effects of probiotic and organic fertilizers as soil amendments on the growth and yield of wheat. *Applied Biological Research*, *23*(2), 157–164. https://doi.org/10.3329/jbs.v29i2.54955

Hussain, S., Mubeen, M., & Karuppannan, S. (2022). Land use and land cover (LULC) change analysis using TM, ETM+, and OLI Landsat images in the district of okara, punjab, Pakistan. *Physics and Chemistry of the Earth*, *126*, 103117. https://doi.org/10.1016/j.pce.2022.103117

Jensen, J. R. (2015). *Introductory digital image processing: A remote sensing perspective* (4th ed.). Prentice-Hall Inc.

Khan, A., Stewart, B. A., Almas, L. K., & Nawab, K. (2017). Impact of variable NPK source on water use efficiency and growth rates of winter grasses (cereals): Wheat, rye, barley and Oats. *African Journal of Agricultural Research*, *12*(49), 3421–3432. https://doi.org/10.5897/AJAR2017.12775

Kumar, A., Sheoran, P., Kumar, N., et al. (2024). Elucidating morphogenic and physiological traits of rice with nitrogen substitution through nano-nitrogen under salt stress conditions. *BMC Plant Biology*, *24*, 908. https://doi.org/10.1186/s12870-024-05569-5

Kuroyanagi, T. (1985). *Senescence of wheat and rice under three temperature regimes* (Master's thesis, Kansas State University, USA).

Li, Y., Tao, F., Hao, Y., Tong, J., Xiao, Y., He, Z., & Reynolds, M. (2022). Wheat traits and the associated loci conferring radiation use efficiency. *The Plant Journal*, *112*(3), 565–582. https://doi.org/10.1111/tpj.15954

Liu, Z., Wang, C., Bi, R., Zhu, H., He, P., Jing, Y., & Yang, W. (2021). Winter wheat yield Estimation based on assimilated Sentinel-2 images with the CERES-Wheat model. *Journal of Integrative Agriculture*, *20*(8), 1958–1968. https://doi.org/10.1016/S2095-3119(20)63483-9

Lu, D., & Weng, Q. (2007). A survey of image classification methods and techniques for improving classification performance. *International Journal of Remote Sensing*, *28*(5), 823–870. https://doi.org/10.1080/01431160600746456

Mohammadi Ahmad Mahmoudi, E., Kamkar, B., & Abdi, O. (2015). Analysis of yield status and its relation with leaf area in wheat fields based on interpolation methods: A case study in army fields, Golestan Province. *Journal of Plant Production Research, 22*(2), 47–69. https://dor.isc.ac/dor/20.1001.1.23222050.1394.22.2.3.2

Monteith, J. L. (1969). Light interception and radiative transfer. In J. D. Eastin, F. A. Haskins, C. Y. Sullivan, & Van C. H. M. Bavel (Eds.), *Physiology of crop plants* (pp. 89–111). ASA.

Monteith, J. L. (1978). Reassessment of maximum growth rates for C3 and C4 crops. *Experimental Agriculture*, *14*(1), 1–5.

Monteith, J. L., & Unsworth, M. H. (2007). *Principles of environmental physics* (3rd ed.). Academic.

Palacios-Rojas, N., McCulley, L., Kaeppler, M., Titcomb, T., Gunaratna, N., Lopez-Ridaura, S., & Tanumihardjo, S. (2020). Mining maize diversity and improving its nutritional aspects within agro-food systems. *Comprehensive Reviews in Food Science and Food Safety*, *19*, 1809–1834. https://doi.org/10.1111/1541-4337.12552

Pearson, R. L., & Miller, L. D. (1972). Remote mapping of standing crop biomass for estimation of the productivity of the shortgrass prairie, Pawnee National Grasslands, Colorado. In *Proceedings of the 8th International Symposium on Remote Sensing of the Environment* (pp. 1357–1381). Ann Arbor, MI.

Qi, J., Chehbouni, A., Huete, A. R., Kerr, Y. H., & Sorooshian, S. (1994). A modified soil adjusted vegetation index. *Remote Sensing of Environment*, *48*(2), 119–126. https://doi.org/10.1016/0034-4257(94)90134-1

Rahemi-Karizaki, A., Khaliliaghdam, N., & Biabani, A. (2021). Predicting time trend of dry matter accumulation and leaf area index of winter cereals under nitrogen limitation by non-linear models. *Plant Physiology Reports*, *26*(3), 443–456. https://doi.org/10.1007/s40502-021-00597-x

Rahimi-Ajdadi, F. (2022). Land suitability assessment for second cropping in terms of low-temperature stresses using Landsat TIRS sensor. *Computers and Electronics in Agriculture*, *200*, 107205. https://doi.org/10.1016/j.compag.2022.107205

Ray, D. K., West, P. C., Clark, M., Gerber, J. S., Prishchepov, A. V., & Chatterjee, S. (2019). Climate change has likely already affected global food production. *PLOS ONE*, *14*(5), e0217148. https://doi.org/10.1371/journal.pone.0217148

RouseJr, J. W., Haas, R. H., Schell, J. A., Deering, D. W., & Harlan, J. C. (1974). *Monitoring the vernal advancement and retrogradation (Greenwave effect) of natural vegetations* (No. NASA-CR-144661). https://ntrs.nasa.gov/api/citations/19750020419/downloads/19750020419.pdf

Saberpour, L., Soufizadeh, S., Mahdavi-Damghani, A., Kambouzia, J., & Ghorbani-Nasrabad, G. (2022). Growth analysis of new cotton (*Gossypium hirsutum* L.) cultivars affected by planting date and nitrogen fertilizer in Golestan. *Environmental Sciences*, *19*, 1–14. https://doi.org/10.52547/envs.2021.23861

Seyam, M. M. H., Haque, M. R., & Rahman, M. M. (2023). Identifying the land use land cover (LULC) changes using remote sensing and GIS approach: A case study at Bhaluka in mymensingh, Bangladesh. *Case Studies in Chemical and Environmental Engineering*, *7*, 100293. https://doi.org/10.1016/j.cscee.2022.100293

Sinclair, T. R. (1986). Water and nitrogen limitations in soybean grain production I. Model development. *Field Crops Research*, *15*, 125–141. https://doi.org/10.1016/0378-4290(86)90082-1

Sinclair, T. R. (2006). A reminder of the limitations in using beer's law to estimate daily radiation interception by vegetation. *Crop Science*, *46*(6), 2343–2347. https://doi.org/10.2135/cropsci2006.01.0044

Soltani, A., & Sinclair, T. R. (2012). *Modeling physiology of crop development, growth, and yield*. CABI.

Su, Z. (1996). *Remote sensing applied to hydrology: The Sauer River Basin study* (Doctoral dissertation). Ruhr University Bochum.

Suliga, J., Bhattacharjee, J., Chormański, J., Van Griensven, A., & Verbeiren, B. (2019). Automatic Proba-V processor: TREX–Tool for raster data exploration. *Remote Sensing*, *11*(21), 2538.

Tao, Z., Wang, D., Ma, S., Yang, Y., Zhao, G., & Chang, X. (2018). Light interception and radiation use efficiency response to tridimensional uniform sowing in winter wheat. *Journal of Integrative Agriculture*, *17*(3), 566–578. https://doi.org/10.1016/S2095-3119(17)61715-5

Thales Alenia Space France (2021). *Sentinel-2 products specification document*.

The Statistical Center of Iran (2021). *Selected results of temporary crops survey, the year 1400*. Presidency of Iran, Plan and Budget Organization. https://www.amar.org.ir/english/Statistics-by-Topic/Agriculture#113281-releases

Tucker, C. J. (1979). Red and photographic infrared linear combinations for monitoring vegetation. *Remote Sensing of Environment*, *8*(2), 127–150. https://doi.org/10.1016/0034-4257(79)90013-0

United Nations Food and Agriculture Organization (FAO) (2019). *FAOSTAT 2019 food and agriculture data*. Retrieved June 1, 2018, from http://faostat3.fao.org

Viña, A., Gitelson, A. A., Nguy-Robertson, A. L., & Peng, Y. (2011). Comparison of different vegetation indices for the remote assessment of green leaf area index of crops. *Remote Sensing of Environment*, *115*(12), 3468–3478. https://doi.org/10.1016/j.rse.2011.08.010

Wang, B., Feng, P., Chen, C., Liu, D. L., Waters, C., & Yu, Q. (2019). Designing wheat ideotypes to Cope with future changing climate in South Eastern Australia. *Agricultural Systems*, *170*, 9–18. https://doi.org/10.1016/j.agsy.2018.12.005

Wiegand, C. L., & Richardson, A. J. (1990). Use of spectral vegetation indices to infer leaf area, evapotranspiration and yield: I. Rationale. *Agronomy Journal*, *82*(4), 623–629. https://doi.org/10.2134/agronj1990.00021962008200030037x

Wiegand, C., Shibayama, M., Yamagata, Y., & Akiyama, T. (1989). Spectral observations for estimating the growth and yield of rice. *Japanese Journal of Crop Science*, *58*(4), 673–683. https://doi.org/10.1626/jcs.58.673

Xiao, D., Liu, D. L., Wang, B., Feng, P., & Waters, C. (2020). Designing high-yielding maize ideotypes to adapt changing climate in the North China plain. *Agricultural Systems*, *181*, 102805. https://doi.org/10.1016/j.agsy.2020.102805

Yu, L., Shang, J., Cheng, Z., Gao, Z., Wang, Z., Tian, L., Wang, D., Che, T., Jin, R., Liu, J., Dong, T., & Qu, Y. (2020). Assessment of cornfield LAI retrieved from multi-source satellite data using continuous field LAI measurements based on a wireless sensor network. *Remote Sensing*, *12*(20), 3304. https://doi.org/10.3390/rs12203304

Yunusa, I. A. M., Siddique, K. H. M., Belford, R. K., & Karimi, M. M. (1993). Effect of canopy structure on efficiency of radiation interception and use in spring wheat cultivars during the pre-anthesis period in a Mediterranean-type environment. *Field Crops Research*, *35*(2), 113–122. https://doi.org/10.1016/0378-4290(93)90144-C

Zadoks, J. C., Chang, T. T., & Konzak, C. F. (1974). A decimal code for the growth of cereals. *Weed Research*, *14*(6), 415–421. https://doi.org/10.1111/j.1365-3180.1974.tb01084.x

Zhu, W., Sun, Z., Huang, Y., Lai, J., Li, J., Zhang, J., Yang, B., Li, B., Li, S., Zhu, K., Li, Y., & Liao, X. (2019). Improving field-scale wheat LAI retrieval based on UAV remote-sensing observations and optimized VI-LUTs. *Remote Sensing*, *11*(20), 2456. https://doi.org/10.1071/CP15236